Effects of Fe substitution on the electronic, transport, and magnetic properties of $ZnGa_2O_4$: A systematic *ab initio* study

Leonardo Pisani, Tulika Maitra, and Roser Valentí
Institut für Theoretische Physik, Universität Frankfurt, D-6 Frankfurt, Germany
(Received 11 January 2006; revised manuscript received 23 March 2006; published 17 May 2006)

We present a density functional study of Fe doped into the tetrahedral and octahedral cation sites of the wide-band-gap spinel $ZnGa_2O_4$. We calculate the electronic structure for different substitutions and discuss the magnetic and transport properties for each case considering different approximations for the exchange-correlation potential. We show that for certain doped cases, significant differences in the predicted behavior are obtained depending on the exchange-correlation potential adopted. Possible applications of the doped systems as magnetic semiconductors are outlined.

DOI: 10.1103/PhysRevB.73.205204 PACS number(s): 71.20.−b, 71.55.−i, 72.25.−b, 71.15.Mb

I. INTRODUCTION

In recent years, spintronics has emerged as one of the most studied fields of research in semiconductor physics because of the possibility of exploiting both the carrier spin and charge degrees of freedom for the storage and transport of information in semiconductor devices.[1] Because of the already existing fabrication technology for III-V semiconductors, the doping of these systems with magnetic ions [especially the cases of Ga(Mn)As and Ga(Mn)N] is being intensively investigated[2] and a large amount of theoretical and experimental work has been done in order to understand the underlying mechanism for the ferromagnetism in these doped semiconductors.[3,4]

Recently, an alternative approach for this phenomenon has been considered[5] by taking a nonmagnetic spinel semiconductor as host material and by doping it with Fe. The spinel structure (stochiometric formula AB_2O_4) with two types of cation sites (tetrahedral A and octahedral B) offers new possibilities of obtaining ferromagnetic order by doping one or both type of cation sites with magnetic ions. First experiments[5] on the solid solution $[ZnGa_2O_4]_{1-x}[Fe_3O_4]_x$ with $x=0.05$, 0.10, and 0.15 showed that long-range magnetic order is induced with Curie temperatures up to 200 K. Similar attempts by Krimmel *et al.*[6] on $Fe_{0.76}In_{2.17}S_4$ revealed, on the contrary, a spin glass state at low temperatures

Along these lines, we investigate the electronic structure of Fe-doped $ZnGa_2O_4$ within density functional theory (DFT) with special emphasis on the magnetic and transport properties. Since the description of these properties may be affected by the choice of the exchange-correlation (XC) potential considered within DFT, we perform a comparative study of the properties by considering two different XC approaches: the local density approximation[7] (LDA) and the generalized gradient approximation (GGA).[8] We observe that though the electronic structure of the parent compound $ZnGa_2O_4$ remains almost unaffected by the change of the XC potential chosen, the kind of Fe substitution (e.g., whether in the A or B site) shows quite different magnetic and transport properties depending on the chosen XC functional.

We will show that the various doping options allow for a variety of interesting behaviors which range from spin-polarized metal to the so-called "transport half-metal." Though both properties are of potential interest for spintronic purposes, we will discuss the speculation that alternative choices of substituent or host compound may improve the quality of these properties.

We have organized the paper in the following way. In Sec. II we present a study of the volume optimization of the parent compound within the LDA and GGA, which sets the reference frame for the doped cases. In the subsequent three sections (Secs. III–V) we analyze the electronic structure properties of Fe-doped $ZnGa_2O_4$ within both XC potentials in three different limits: namely, Fe doped in the Zn position, Fe doped in the Ga position, and Fe doped in both Zn and Ga positions, respectively. Finally in Sec. VI we present a summary of our calculations with a comparison to the available experimental data and conclude with suggestions for some possible future experiments.

II. PARENT COMPOUND

A. Computational details

We have performed DFT calculations using the full-potential linearized augmented-plane-wave (LAPW) code WIEN2k.[9] In our calculations, we chose APW+lo as the basis set. The atomic sphere radii were chosen to be 1.8 a.u. for Zn, Ga, and Fe and 1.6 a.u. for O. Expansion in spherical harmonics for the radial wave functions was taken up to $l=10$, and the charge densities and potentials were represented by spherical harmonics up to $L=6$. For Brillouin-zone (BZ) integrations we considered a 60-**k**-point mesh in the irreducible wedge and the modified tetrahedron method was applied.[10]

B. Volume optimization

$ZnGa_2O_4$ crystallizes in a normal spinel structure [space group $Fd\bar{3}m$ (227)] with the primitive (rhombohedral) unit cell containing two formula units with Zn, Ga, and O at the positions $(1/8,1/8,1/8)$, $(1/2,1/2,1/2)$, and (u,u,u), respectively (where $u=1/4$ corresponds to a perfect spinel structure). Zn is sorrounded by a tetrahedral environment of

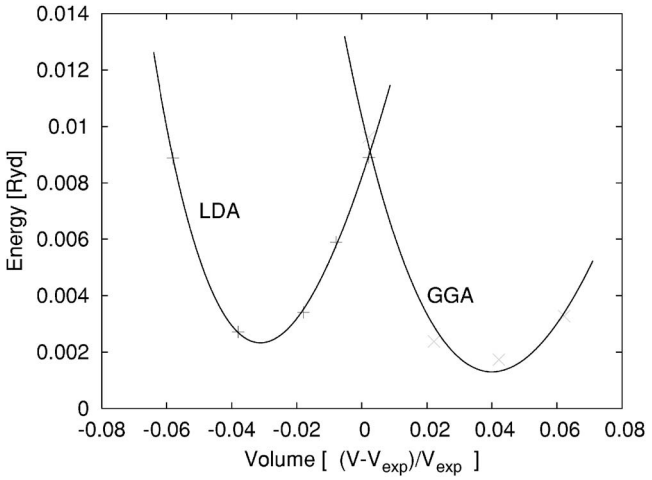

FIG. 1. Volume optimization curves for the LDA and GGA XC functionals. The energy scale has been made arbitrary for plotting reasons, and the volume scale measures the relative value respect to the experimental one.

oxygen atoms while Ga sits on an octahedral position. In order to adopt a reliable approximation for the XC potential in the description of the parent compound, we performed a full volume optimization within two widely used parametrizations of the XC functional: namely, the LDA (Ref. 7) and the GGA (Ref. 8) approaches. For each selected volume we also considered the relaxation of the internal coordinate of oxygen (u parameter) as allowed by the symmetry in the space group 227, by using the damped Newton dynamics method, until a force value smaller than 1 mRyd/a.u. was reached. The energy minimum of the various selected volumes defines then the optimal volume. Figure 1 shows the total electronic energy as a function of the volume of the rhombohedral unit cell for the LDA and GGA ($V=\frac{1}{4}a^3$ where a is the conventional cubic cell parameter).

The optimized lattice constant, whose experimental value[11] is $a=8.334$ Å, is found to be underestimated in the LDA by about 1% and it is overestimated in the GGA by about 1.5%. In Table I we show a comparison of tetrahedral (Zn-O) and octahedral (Ga-O) distances between the optimized ones and the experimental ones. Note that the experimental values are underestimated by the LDA and overestimated by the GGA. This kind of behavior is generally not unexpected when adopting LDA or GGA in the description of semiconductors. For instance, in a recent *ab initio*[12] study of spinel $ZnAl_2O_4$, the LDA lattice constant underestimation was found to be of 1.1%. The origin of the LDA and GGA shortcomings may be ascribed to the inability of both approximations to describe properly the binding due to long-range forces like the van der Waals interaction (apart from the inaccuracy concerning exchange and correlation). In contrast, optimization of the u parameter for $ZnGa_2O_4$ converges to 0.3861 within the LDA and 0.3866 within the GGA, both in good agreement with the experimental value of 0.3867.

TABLE I. Optimized and experimental tetrahedral and octahedral distances.

	LDA	GGA	Expt.
Zn-O (Å)	1.943	1.997	1.974
Ga-O (Å)	1.975	2.018	1.991

We have also estimated the residual and less important discrepancies due to the neglect of the zero-point and thermal motion of the atoms. Assuming the cubic spinel to be an isotropic three-dimensional harmonic oscillator with a spring strength given by the curvature of the energy versus lattice constant function, we estimate the ground-state length fluctuation to be 0.019 Å within the LDA. This represents a deviation of about 0.2% with respect to the classical adiabatic value. The thermal expansion from zero to room temperature is expected to produce an effect on the lattice parameter less than 0.1%, as can be inferred from the data of Josties *et al.*;[11] therefore, these corrections fall within the inaccuracy of the XC approximations used here.

From the fit of the energy-volume curves of Fig. 1 to the Murnaghan equation of state[13] we extract a bulk modulus for $ZnGa_2O_4$ of 217 GPa within the LDA and 146 GPa within the GGA. Structure optimizations for the spinels $ZnAl_2O_4$ and $ZnGa_2O_4$ have been performed in the past within the framework of the shell model,[14] providing a bulk modulus of 273 and 237 GPa, respectively. Recently Levy *et al.*[15] have measured the bulk modulus of $ZnAl_2O_4$ to be 202 GPa, well below the value obtained by the shell model (273 GPa). Therefore, assuming that the shell-model bulk modulus is affected by the same amount of discrepancy for both $ZnAl_2O_4$ and $ZnGa_2O_4$ and since our calculated values for $ZnGa_2O_4$ are lower than that of the shell model, we expect our results to be in a better agreement to experiment than the shell model result.

We conclude from the previous comparison that the gradient correction to the LDA as implemented in the GGA does not produce a significant improvement upon the LDA itself as far as the host compound is concerned. However, in the following sections we will see that upon Fe substitution the LDA and GGA outcomes may turn out to be quite different.

C. Electronic structure

In this section we present the density of states (DOS) and band structure of the parent compound within the LDA and GGA. In Fig. 2 both properties are shown only for the LDA approach since no significant modification is observed within the GGA. These results prove to be in good agreement with previous calculations.[16]

The spinel $ZnGa_2O_4$ is a semiconductor with a measured band gap of about 4.0 eV.[17] At the Γ point the band gap is calculated here to be 2.7 eV which reminds us of the renowned tendency of the LDA to underestimate the electronic band gap. No significant improvement in the gap value is detected within the GGA. The DOS shows the valence band to be mainly of O character with a peaked Zn weight due to the full d orbital shell. The Ga d states are confined below −10 eV (not shown) and strongly atomic like.

It is important here to point out the dispersive feature of the band structure at the Γ point above the Fermi level which has mainly Ga and O character. The associated effective

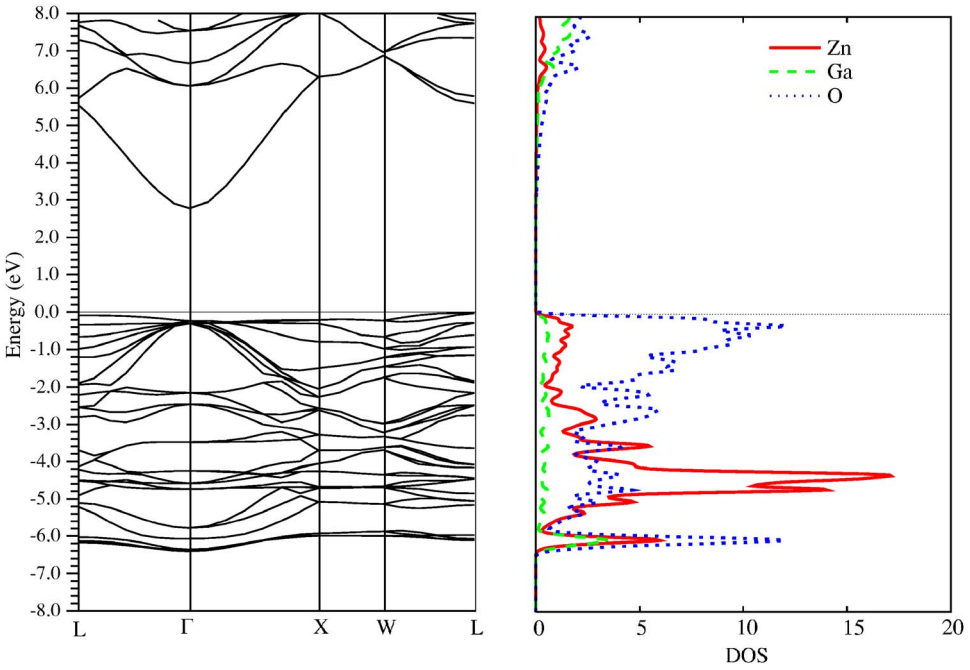

FIG. 2. (Color online) Band structure and decomposed density of states for $ZnGa_2O_4$ within the LDA. The path chosen in the Brillouin zone is $L=(1/2,1/2,1/2)$, $\Gamma=(0,0,0)$, $X=(0,1,0)$, and $W=(1/2,1,0)$ in units of $2\pi/a$. The DOS is given in units of states per eV and per atom in all the figures.

mass is calculated to be 0.28 times the electron rest mass and is rather isotropic; therefore, doping with a magnetic ion may open the possibility for a high-mobility electronic current which simultaneously might be fully spin polarized, as we will discuss in the next paragraphs. Finally, recalling that the DOS weights are given within the atomic sphere radii considered in the APW+lo basis, the smallness of the weight of the dispersive s band at Γ (Fig. 2, right panel) is due to the large extension of the $4s$ state outside the sphere (interstitial region).

III. Fe DOPED INTO THE *A* POSITION

Substitution of Fe in one of the two Zn sites of the rhombohedral unit cell removes the inversion symmetry from the space group $Fd\bar{3}m$ and reduces it to the maximal subgroup $F\bar{4}3m$ (space group 216). In addition, the original eight equivalent oxygen positions are now split in two nonequivalent sets (Wyckoff position $16e$).[18] Defining the doping concentration with respect to the total number of tetrahedral sites, this new structure corresponds to a 50% Fe doping. In a tetrahedral crystal field, the Fe d levels are split into energetically lower e_g states and upper t_{2g} states.

We have calculated the electronic structure for this system within the spin-polarized versions of the LDA and GGA. Both approaches lead to very similar results; therefore, we discuss here the LDA results and comment on quantitative differences with respect to the GGA.

In Fig. 3 the density of states and band structure are shown for the spin-polarized LDA case (LSDA). Since no major modification with respect to the parent compound is observed as far as the Zn and Ga weights are concerned and the size of the band gap (2.7 eV) remains unchanged, we show in the DOS only the Fe and O weights (Fig. 3 right panels).

Note the full inclusion of the iron antibonding $3d$ majority (spin-up) states within the band gap of the parent compound (Fig. 3, upper right panel), while the $3d$ minority (spin-down) states hybridize with the highly dispersive s band at the Γ point (Fig. 3, lower right panel). In a previous work by Nonaka *et al.*[19] the authors did a molecular orbital calculation of one Fe atom doped into the Zn position of a $ZnGa_2O_4$ cluster and found the Fe d states to be located in the band gap of the host cluster.

Due to the absence of any d character at the Fermi level for the majority states, we may therefore argue that the conduction properties of this compound are strongly spin dependent. In fact, the s conduction in the spin-down channel may be hindered by the presence of the relatively localized d states which are instead absent in the spin-up channel. The situation partially resembles the case of transition metal ferromagnets like iron, cobalt, and nickel, where the Fermi level lies in the $d\downarrow$ band but the effective spin polarization in transport is positive, due to the more mobile $4s(\uparrow)$ electrons.

The exchange splitting is comparable in size with the band gap (2.7 eV) and much larger than the crystal field splitting (0.8 eV). The oxygen hybridization is more pronounced in the majority-spin bands than in the minority ones, as indicated by the larger weight of O in the majority-state valence band. This is ascribed to the t_{2g} symmetry of the filled majority states which in a tetrahedral ligand field have a σ bonding with oxygen, in contrast to the minority t_{2g} states which are here almost empty.

According to an ionic picture, iron in the A position is expected to assume a $3d^6$ (Fe^{2+}) configuration in a high-spin state with a magnetic moment of $4\mu_B$. The calculated total magnetic moment per unit cell is $4.01\mu_B$ and is distributed mainly among Fe, O(1), and interstitial contributions in a proportion $3.19\mu_B$, $0.08\mu_B$, and $0.47\mu_B$, respectively. Recalling that the iron muffin-tin radius considered in the calculation is 0.95 Å, we expect the interstitial magnetic moment to

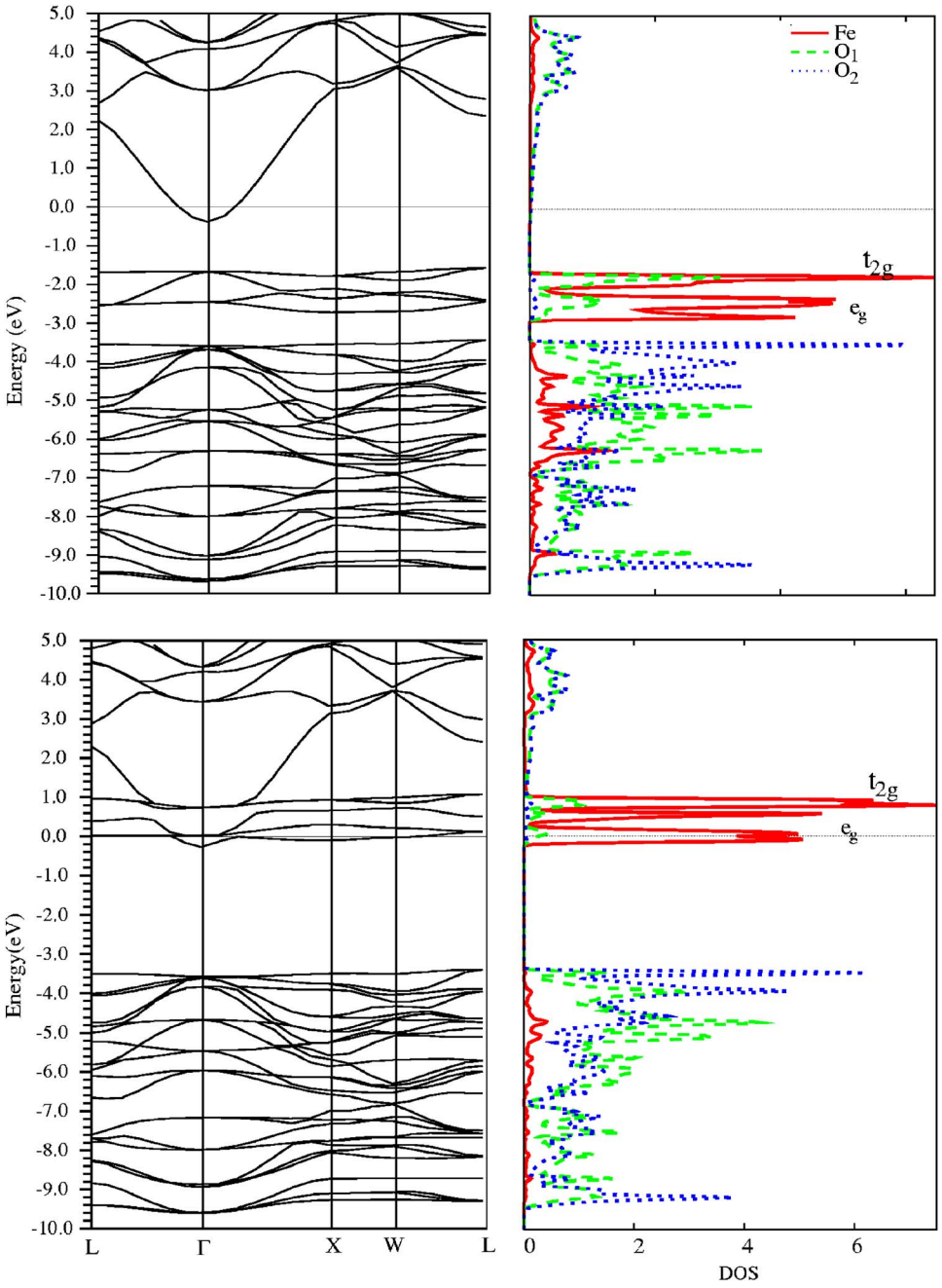

FIG. 3. (Color online) Band structure and density of states for Fe doped into the A site of $ZnGa_2O_4$ within LSDA. Upper panels: majority states (spin up). Lower panels: minority states (spin down). Recall that the DOS weights are given within the atomic sphere radii. Therefore the small s weight at E_F in the DOS panel is due to the large extension of the $4s$ state outside the sphere (interstitial region).

be mainly due to the d orbital tails leaking out of the atomic sphere.

Calculations within the GGA give a total magnetic moment per unit cell of $4.03\mu_B$, and the Fe, O(1), and interstitial moments are $3.28\mu_B$, $0.07\mu_B$, and $0.46\mu_B$, respectively. Looking at the Fe moment one clearly sees a larger degree of localization within the GGA with respect to the LDA. To confirm this, we examine the total amount of charge in the atomic spheres and we find that it is increased in the GGA respect to the LDA. No other important differences have been detected.

Because of the highly localized nature of iron d states, one may argue about the importance of inclusion of orbital on-site correlations on top of a mere LSDA approach. We have performed a LDA+U calculation and considered two different versions of the double-counting correction—namely AMF ("around mean field") by Cyzyk and Sawatzky[20] and FLL (full localized limit) by Anisimov *et al.*[21] (U=4.5 eV and J=1 eV). No relevant modification respect to the LSDA case has been noted in both cases. In fact, the LDA+U method aims at producing a fully orbitally polarized ground state by opening a gap between the occupied and nonoccupied states. In the present case both versions result only in increasing the crystal field splitting e_g-t_{2g} of the minority states just above the Fermi level pushing the upper three t_{2g} bands further above.

It is also interesting to note that the ionic radii of Zn^{2+} and Fe^{2+} in a tetrahedral coordination are very similar—namely, 0.6 and 0.63 Å. As a consequence, the global (lattice parameter) and local (tetrahedrally coordinating oxygen) readjust-

ment of the structure due to the substitution is expected not to bring major modification to the electronic properties above discussed. This is in fact confirmed within both the GGA and LDA calculations where the force values acting on the O and Ga atoms are around 1 mRyd/a.u. and therefore negligible. This also confirms the minor importance of the differences between the two approaches when Fe is substituted in a tetrahedral site. In the next section we shall see that important differences appear when Fe is substituted in an octahedral site.

To determine the ground-state magnetic order of this systems we performed an antiferromagnetic calculation, doubling the present unit cell. Comparing the total energies of antiferromagnetic and ferromagnetic configurations we found that the ferromagnetic state is lower in energy by about 61 meV. This state was also predicted to be the ground state in this doping limit from a proposed phenomenological model in an earlier communication by two of us.[22]

IV. Fe INTO THE *B* POSITION

Substituting iron into one of the four Ga sites of the primitive unit cell of $ZnGa_2O_4$ causes the lattice symmetry to lower from cubic (space group 227) to the rhombohedral space group $R\bar{3}m$ (166). In this group, the eight equivalent oxygen positions of the parent group (Wyckoff position 32*e*) split into 2*c* and 6*h* positions, with the latter being the oxygen atoms octahedrally coordinating iron. In an octahedral environment, the 3*d* orbitals of Fe are split into energetically lower t_{2g} and higher e_g manifolds.

For the present case we find a significant difference between the LDA and GGA outcomes. In fact we performed volume optimizations for both approaches and we find that LDA produces as a ground state an intermediate spin state for Fe; i.e., the unit cell magnetic moment is calculated to be $1\mu_B$. Therefore, within a simplifying ionic picture, only the t_{2g} manifold is populated with three electrons in the up sector and two in the down one, resulting in a Fe^{3+} oxidation state in the intermediate-spin state 1/2.

On the contrary, the GGA describes Fe in a high-spin state with a unit-cell magnetic moment equal to $5\mu_B$. The reason for this strong difference may be connected to the element Fe itself. According to the LDA, Fe is predicted to be nonmagnetic and with a fcc structure while within the GGA the correct magnetic bcc structure is found.[23] Therefore we may expect the GGA to be more reliable than the LDA for the *B*-site doping.

Another reason in favor of the GGA is the end compound zinc ferrite, $ZnFe_2O_4$, where Fe replaces all the Ga atoms. Recent band-structure calculations[24] have shown that zinc ferrite behaves as a metal within the LDA and as an antiferromagnetic insulator with a small gap within the GGA. The transport gap has been measured to be 0.2 eV (Ref. 26) in support of the GGA outcome.

We can understand the strong discrepancy between the LDA and GGA with the help of the Table I and recalling the typical Fe-O distances for the high-spin state of Fe (2.2–2.3 Å) and for the low-spin state (1.8–1.9 Å). We see that the Ga-O LDA distance is a low-spin distance; therefore after substitution and after volume optimization the Fe-O distance, which increases only by 1%–2%, will remain of the low-spin state type. On the contrary the GGA Ga-O distance is much closer to the high-spin region and thus after volume optimization Fe will be in a high-spin state.

In Fig. 4 we present the GGA band structure and DOS. As in the previous case, the band gap of the parent compound remains approximately unchanged (~2.7 eV). The majority-spin *d* states of iron (Fig. 4, upper panel) are fully occupied, of which the t_{2g} subband completely hybridizes with the oxygen valence band and the e_g antibonding states set the Fermi level. Concerning the minority states (Fig. 4, lower panel), those antibonding with oxygen are completely empty implying that the Fe is in an oxidation state 3+.

From Fig. 4 we find thus a zero-temperature insulator with a band gap of 0.4 eV. It is interesting to compare this band gap with that of the end compound $ZnFe_2O_4$ where within the GGA it is calculated to be one order of magnitude less.[24] This can be ascribed to the direct cation-cation bonding in the case of $ZnFe_2O_4$. Since the Fe atoms are at the center of edge sharing oxygen octahedra, the t_{2g} orbitals are able to directly overlap among each other producing a widening of the t_{2g} bands due to hybridization. This causes the minority t_{2g} bands just above the Fermi level to become closer to E_F with a consequent reduction of the band gap. The spin exchange splitting for the present doped system is of about ~2.5 eV, similar to the previous case, but the crystal field splitting is around ~1.8 eV, more than the double as for the previous case.

The unit-cell magnetic moment, which is calculated to be $5.0\mu_B$ within the GGA, is distributed mostly among the Fe muffin-tin sphere, interstitial region, and oxygen muffin-tin sphere in a proportion $3.93\mu_B$, $0.40\mu_B$, and $0.10\mu_B$, respectively.

Note that in this case, at the Γ point the *d* band in the minority sector remains above the Fermi level due to the oxidation state of Fe (3+) which leaves the minority antibonding *d* states unpopulated. Moreover, due to the larger crystal field effect, only the e_g bands hybridize with the 4*s* band at Γ while the t_{2g} states are pushed down just above the Fermi level. Therefore, if we were to reproduce a situation similar to the *A*-site case (see previous section) in which the 4*s* band should be at the Fermi level, we would need a transition metal in a 3+ oxidation state with nine electrons in the *d* shell—namely, Zn^{3+}—which does not exist.

In order to determine the ground-state magnetic order, we compared the total energies of ferromagnetic and antiferromagnetic alignments of the iron spin. For this purpose we doubled the primitive unit cell into a tetragonal one containing 4 Zn, 6 Ga, 2 Fe, and 16 O atoms. We have then considered an antiferromagnetic arrangement, where the spins of the two nonequivalent Fe atoms in the tetragonal unit cell are antiparallel to each other. This type of magnetic arrangement gives us planes of ferromagnetically aligned ions with an interplane antiferromagnetic coupling. Comparing the total energy between this alignment and the ferromagnetic one, we find the former already to be lower in energy by 1 eV with respect to the latter.

In conclusion, we find that doping Fe into a Ga site in a concentration of 25% results in an antiferromagnetic semi-

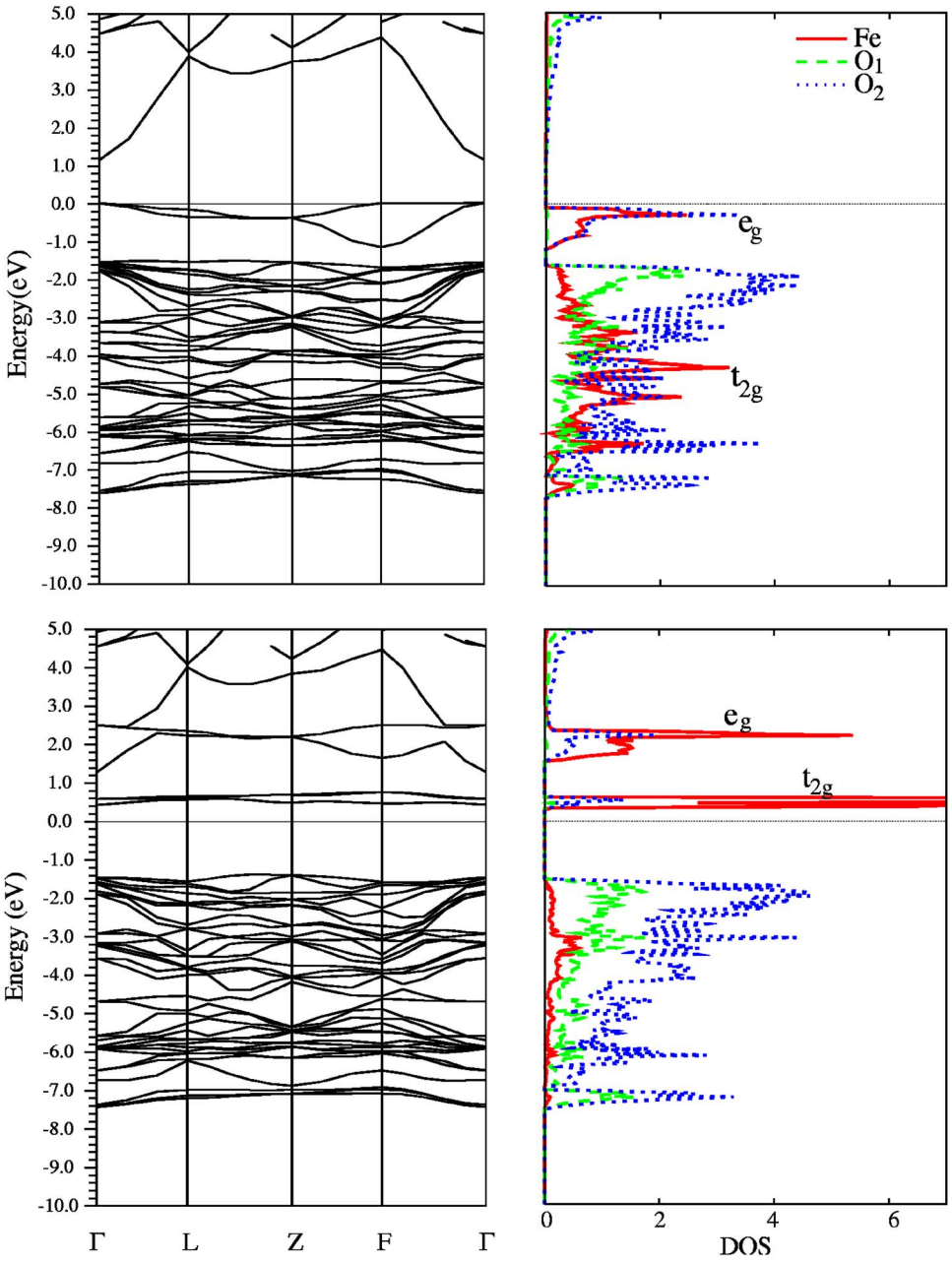

FIG. 4. (Color online) Band structure and density of states for Fe in the B site of $ZnGa_2O_4$ within the GGA. Upper panels: majority (spin-up) manifolds. Lower panels: minority (spin-down) manifolds. The path chosen in the Brillouin zone is $\Gamma=(0,0,0)$, $L=(0,1/2,0)$, $Z=(1/2,1/2,1/2)$, and $F=(1/2,12,0)$ in units of the trigonal reciprocal-lattice vectors.

conductor at zero temperature which could show conducting properties with increasing temperature. Namely, the t_{2g} minority states can be thermally populated and produce a spin-polarized current. But due to flatness of the t_{2g} bands, just above the Fermi level, the mobility of the carriers would be very low. On the contrary, due to the strong difference in the hybridization of e_g and t_{2g} states with oxygen, the e_g bandwidth is much larger than the t_{2g} one, as clearly seen from the band structure shown in Fig. 4. Therefore, setting the Fermi level into the majority e_g manifold would induce a half-metallic behavior with a fully spin-polarized current. This can be achieved by doping, for instance, with Mn instead of Fe.

V. Fe DOPED INTO *A* AND *B* POSITIONS

The third case that we considered in this study is the doping of iron in both sites A and B in a ratio 1:2 (Fe_A:Fe_B) and in a total concentration of 25%. Accordingly, we double the rhombohedral primitive unit cell of the parent compound into a tetragonal unit cell containing 4 Zn, 8 Ga, and 16 O atoms. Defining the doping concentration with respect to the total number of occupied cation sites, 25% doping of Fe (in both A and B sites) corresponds to substituting 1 Zn atom with 1 Fe atom and 2 Ga atoms with 2 Fe atoms in the tetragonal unit cell. Two inequivalent structures turn out to be consistent with this sort of doping [Figs. 5(i) and 5(ii)], both belonging to the space group Pm (6). In the structure (i) the Fe_A and Fe_{B2} atoms form zigzag chains with O atoms in between them (e.g., Fe_A-O-Fe_{B2}-O-Fe_A) along the a direction and the Fe_{B1} atoms are connected to the Fe_A through O along the c direction. The angles Fe_A-O-Fe_{B1} and Fe_A-O-Fe_{B2} are equal to 121°, and there is no direct path between Fe_{B1} and Fe_{B2}. In the structure (ii) the two Fe_B are crystallographically equivalent and their distance is much shorter (2.92 Å) than

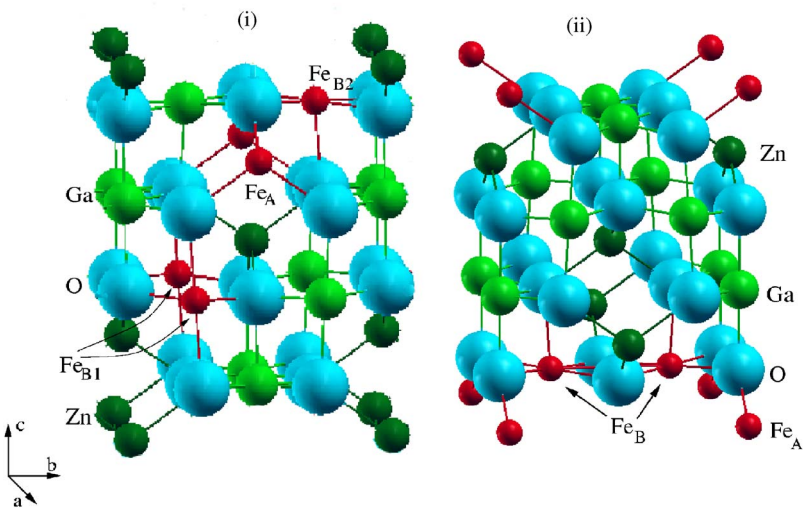

FIG. 5. (Color online) Crystal structures considered for Fe doped in the *A* and *B* positions in a concentration of 25% (see text). In both cases Fe_A is situated at the corners of the unit cell and in case (i) the Fe_B atoms (Fe_{B1}-Fe_{B1}/Fe_{B1}-Fe_{B2}) distance is 5.83 Å while in case (ii) the Fe_B atoms distance is 2.92 Å.

in the case (i) (5.83 Å); therefore, direct metal-metal bonding is realized in this situation.

To clarify the role of the on-site correlation typical of the transition metal ions for the present case we have performed calculations within the LDA+U potential, besides the GGA one. We will present here only the LDA+U (Ref. 21) results since no major differences have been detected from the GGA outcome. (The LDA calculation has not been taken in consideration because of the failure of LDA in describing Fe in the *B* case.) The values considered for the Hubbard and exchange parameters *U* and *J* are 4.5 and 1 eV, respectively.

In Fig. 6 we present the spin-polarized DOS and related band structure within L(S)DA+U for the structure of Fig. 5(i). We have adopted a ferrimagnetic alignment of the Fe spins; specifically, the Fe_A spins are up and Fe_B spins are down. Therefore the majority states of Fe_A are spin up and the majority states of Fe_B are spin down. The upper panel of the Fig. 6, which shows the band structure and DOS of the spin-up species, will contain the Fe_A majority states and the Fe_B minority states, while the lower panel of Fig. 6 (spin-down species) will contain the Fe_A minority states as well as the Fe_B majority states.

In Fig. 7 we present a simplified schematic energy level diagram to show the approximate location of the *d* bands of Fe_A and Fe_B.

As the two Fe_{B1} and Fe_{B2} bands have rather similar features, we show in Fig. 6 (right panel) the sum of the two Fe_B weights. In the energy range from −10 eV to about −3 eV the host compound valence band is found to have predominantly oxygen character. In this range the Fe-O hybridization occurs mainly in the Fe_B spin-down bands (see lower panel of Fig. 6) and less importantly in the Fe_A states. In the interval from −3 eV to −1 eV the impurity bands are clearly visible: the spin-up bands (see upper panel) show the Fe_A e_g nonbonding and the t_{2g} antibonding states in the order of increasing energy, and the spin-down bands (lower panel) are mainly Fe_B e_g antibonding states spanning the same energy range. At the Fermi level (see also Fig. 7) the Fe_A e_g spin-down band (lower panel), due to the lowering of the point symmetry at the *A* site, splits into an almost fully occupied band and an empty e_g band at about 1.5 eV above the Fermi level. In the upper panel, the Fe_B t_{2g} spin-up bands are found slightly occupied and above them we distinguish the empty Fe_B e_g states. In the same energy range we find in the lower panel the split e_g spin-down bands and the t_{2g} bands of Fe_A. The effect of *U* will be discussed in the next paragraph.

According to an ionic picture, the oxidation states of Fe_A and Fe_B would be 2+ and 3+, respectively. However, due to the small overlap of opposite spin bands at the Fermi level, the ionic values are slightly changed (increased for Fe_A and reduced for Fe_B). In fact the magnetic moment of the unit cell is found to be $-5.97\mu_B$, while in the case of an ionic picture it would be $-6\mu_B$, since the magnetic moments of Fe_A and Fe_B's are, respectively, $4\mu_B$ and $-5\mu_B$ [4+2(−5)]. A comparison with magnetite, which represents the end compound for Fe doping in both *A* and *B* sites and has a fully inverted spinel structure—i.e., $(Fe_A^{3+})(Fe_B^{3+}Fe_B^{3+})O_4$—tells us that in the compound (i) the Fe valence states are beginning to invert; namely, the Fe_A increases its oxidation state towards 3+ and Fe_B decreases it to 2.5+.

An important point concerning the band structure shown in Fig. 6 is the role of the Hubbard *U* in the semimetal picture. Since the Hubbard *U* represents the on-site Coulomb correlations and no intersite Hubbard *V* has been included in our calculations, no effect on the electronic structure at the Fermi level of Fig. 6 is expected by varying *U* since it contains two sets of bands originating from two different sites. In fact, we performed a further calculation changing the *U* value of Fe_A and Fe_B and, as expected, only a relative shift respect to the Fermi level is found for occupied (downwards shift) and unoccupied (upwards shift) states, leaving the relative position of the up and down bands at the Fermi level unchanged. The main effect of the Hubbard *U* is thus to open a gap between occupied and unoccupied states and to increase the crystal field splitting which is already taken into account by a LDA-only description. Therefore, in the case of Fe_B sites, the Hubbard *U* just adds to the exchange interaction constant since the down states are fully occupied and the up states are almost completely empty, while in the case of the Fe_A site, due to the presence of Fe_B as second nearest neighbor, which further splits the degeneracy of the e_g bands, the Hubbard *U* transforms this split into a sizable gap. In a

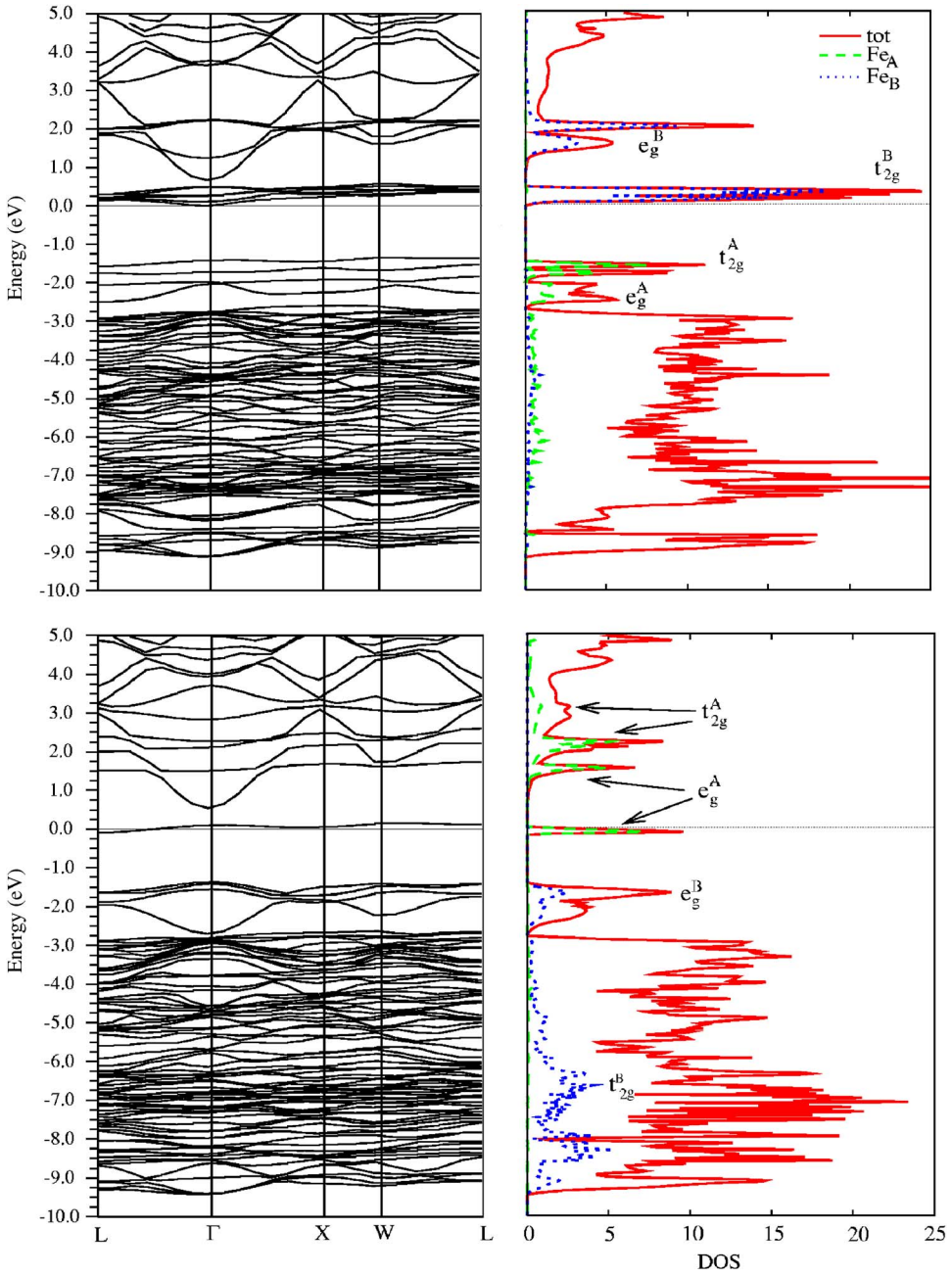

FIG. 6. (Color online) Band structure (left panel) and total and decomposed density of states (right panel) (color online) for the structure of case Fig. 5(i) within LDA+U with $U=4.5$ eV and $J=1$ eV. Shown are the results for the up-spin manifold (upper panel of the figure) and the down-spin manifold (lower panel of the figure).

pure LSDA treatment the Fe_A e_g down bands would not show a relevant splitting, thus overlapping with Fe_B t_{2g} up bands and the conduction band would not have an almost pure spin polarization nature as in the present case.

Another important effect to take into account is the unit-cell expansion or contraction due to the replacement of some of the Zn and Ga atoms with Fe. In this case we cannot describe Fe_A and Fe_B as in a 2+ and 3+ oxidation states, respectively, since the compound is partially inverted, and thus we cannot expect minor changes of the structure due to the similar ionic radii of Zn^{2+} with Fe^{2+} and Ga^{3+} with Fe^{3+}, as seen in the previous cases. To have an idea of the structural modification, we recall that the ionic radius of Fe^{3+} in the A site is 0.49 Å and it is 0.78 Å for Fe^{2+} in the B site, while the Zn^{2+} and Ga^{3+} ionic radii are, respectively, 0.6 Å and 0.62 Å. We shall discuss the atomic forces for the present structure at the end of this section.

Finally, we can attempt a rough estimation of the ferrimagnetic ordering temperature by exploiting the analogy with magnetite Fe_3O_4. The latter is known to have the highest ferrimagnetic temperature of 858 K. Considering the expression $k_B T_N \simeq 4\sqrt{2} J_{AB} S_A S_B$,[25] where the coupling constant J_{BB} between two B sites and between two A sites (J_{AA}) has been neglected with respect to the magnitude of J_{AB}, one obtains a good estimation of the Néel temperature for magnetite when $J_{AB} \simeq 19$ K. In our case we assume a simple multiplicative rescaling effect of the magnetic ion concentration on the geometric factor $4\sqrt{2}$ and that the exchange constant does not depend on the absolute spin value of the two Fe. Calculating the total energy differences between the fer-

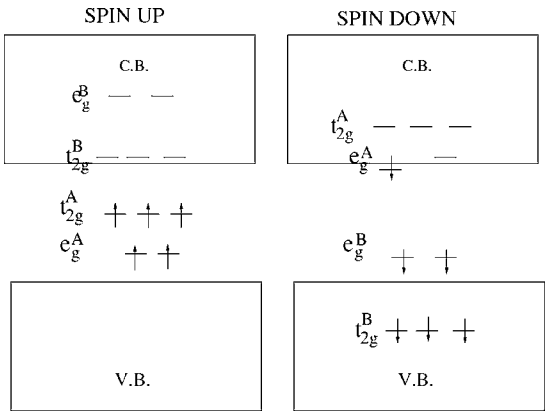

FIG. 7. Schematic picture showing the relative positions of Fe_A and Fe_B levels in the band structure of the doped $ZnGa_2O_4$ for the crystal structure of Fig. 5. C.B. and V.B. denote the conduction and valence bands of the host compound.

romagnetic and ferrimagnetic alignment of the Fe spins we obtain an exchange constant J_{AB} value of 25 K which by means of the above formula provides us with a transition temperature of 260 K.

We now discuss the case Fig. 5(ii). It is important to note that the driving mechanism here is due to the Fe_B-Fe_B bonding while in case (i) Fe_B are connected to Fe_A through oxygen and no direct Fe_B-Fe_B bonding is realized.

Figure 8 shows the total and decomposed densities of states within L(S)DA+U of both spin species. The magnetic ground state is found to have antiferromagnetic order between Fe_A (majority spin ↑) and Fe_B (majority spin ↓). The spin-up bands (upper panel) of Fe_A and Fe_B are completely filled and confined in the valence band which has a charge gap of about 1 eV with respect to the down-spin manifold. The spin-down bands (lower panel) are at the Fermi level for both Fe_A and Fe_B, indicating a mixed-valence oxidation state. Similar to case (i), the point symmetry at the Fe_A site is reduced by the presence of next-nearest-neighbor Fe_B which leads to the splitting of the Fe_A e_g band into two nondegenerate bands. One of them is completely empty (the peak just above E_F) and the other partially filled (the peak at E_F). The remaining charge partially occupies the antibonding spin up Fe_B bands which have t_{2g} symmetry. The system thus prefers to assume a partially inverted structure with respect to the fully inverse one of magnetite where only Fe_B antibonding states are at the Fermi level. Due to the shorter Fe_B-Fe_B distance of 2.92 Å, the metal-metal bonding produces a larger bandwidth of Fe_B states at E_F as well as a higher electronic population of Fe_B states in (ii) with respect to (i) as is clear by comparison of the DOS of the minority Fe_B states between case (i) and (ii) (see Figs. 6 and 8, upper panel). We may therefore conclude that the degree of inversion in (ii) is larger than that in (i) and we may then argue that the driving mechanism in the inversion of magnetite is due to the direct cation(B)-cation(B) bonding.

Moreover, from the band structure (Fig. 8) it is clear that the spin-down Fe_A band at E_F (lower panel) is much less dispersive than the spin-up Fe_B band (upper panel), resulting in a Mott-Hubbard-like behavior of the *A* site. Therefore, we find here a particular kind of half-metallic behavior of the system with respect to the conventional full spin-polarized half-metals. In fact, both spin species are here present at the Fermi level but only one of them ($\downarrow t_{2g}$ Fe_B states) is significantly conducting while the other ($\uparrow e_g$ Fe_A states) is strongly localized. This kind of system is called *transport* half-metal as opposed to a conventional half metal where the spin polarization (P) is 100%. We calculated the value of P for the present case according to the definition[27] $P_n = \frac{N_\uparrow v_\uparrow^n - N_\downarrow v_\downarrow^n}{N_\uparrow v_\uparrow^n + N_\downarrow v_\downarrow^n}$, where N is the density of states at the Fermi level for the two spin species and v the respective Fermi velocity. From the calculated band structure and DOS we derive a value of P_1 equal to 35% and of P_2 equal to 81%. Since the bulk current is proportional to $N(E_F)v_F^2$, the P_2 value implies that 90.5% of the current is carried by the spin ↑ electrons, (namely the minority spins of Fe_B) and a *transport* half-metal is clearly realized.

However, we should recall that the charge carrier concentration in this case is less than that in magnetite and therefore the metallicity of this system is poorer than the one of magnetite.

Finally, some considerations on the stability of the proposed structures should be done at this stage. Due to the lack of implementation of atomic forces calculation for an LDA+U potential in the WIEN2k code and aware of the fact that the inversion issue in spinels is not intrinsically due to on-site Hubbard effects, we have estimated the instability of structures (i) and (ii) respect to inversion by evaluating atomic forces within the GGA potential. The structures (i) and (ii) considered here are the GGA optimized ones and have not been relaxed after replacement of Zn and Ga with Fe. In Table II we show the moduli of the forces acting on Fe_A, Fe_B, and the oxygen connecting them, which are the most significant ones. Note the difference in magnitude between cases (i) and (ii) for Fe_A and oxygen due to the larger degree of inversion of (ii) respect to (i). Comparing the force directions (not shown in the table) we see that the distance between Fe_A and oxygen has to become shorter, testifying to the tendency of both structures to invert. Clearly the structure (ii) is significantly more unstable than the structure (i).

VI. CONCLUSIONS

In conclusion, we have performed a systematic *ab initio* study of Fe-doped $ZnGa_2O_4$ to investigate the effect of Fe substitution on the electronic structure of the parent spinel compound $ZnGa_2O_4$. For an accurate account of the magnetic and transport properties we considered various exchange correlation functionals and we observed that the electronic properties of the doped system depend significantly on the exchange-correlation functional used, especially when Fe is doped on the *B* cation site or on both *A* and *B* cation sites of the spinel compound. Whereas in the case of Fe doped in the *A* site both the LDA and GGA give qualitatively the same results (close to an ionic picture), *B*-site doping leads to a different ground-state spin of Fe within the LDA and GGA. During the course of this study we also tried to explore the possibilities of obtaining a strongly polarized half-metallic

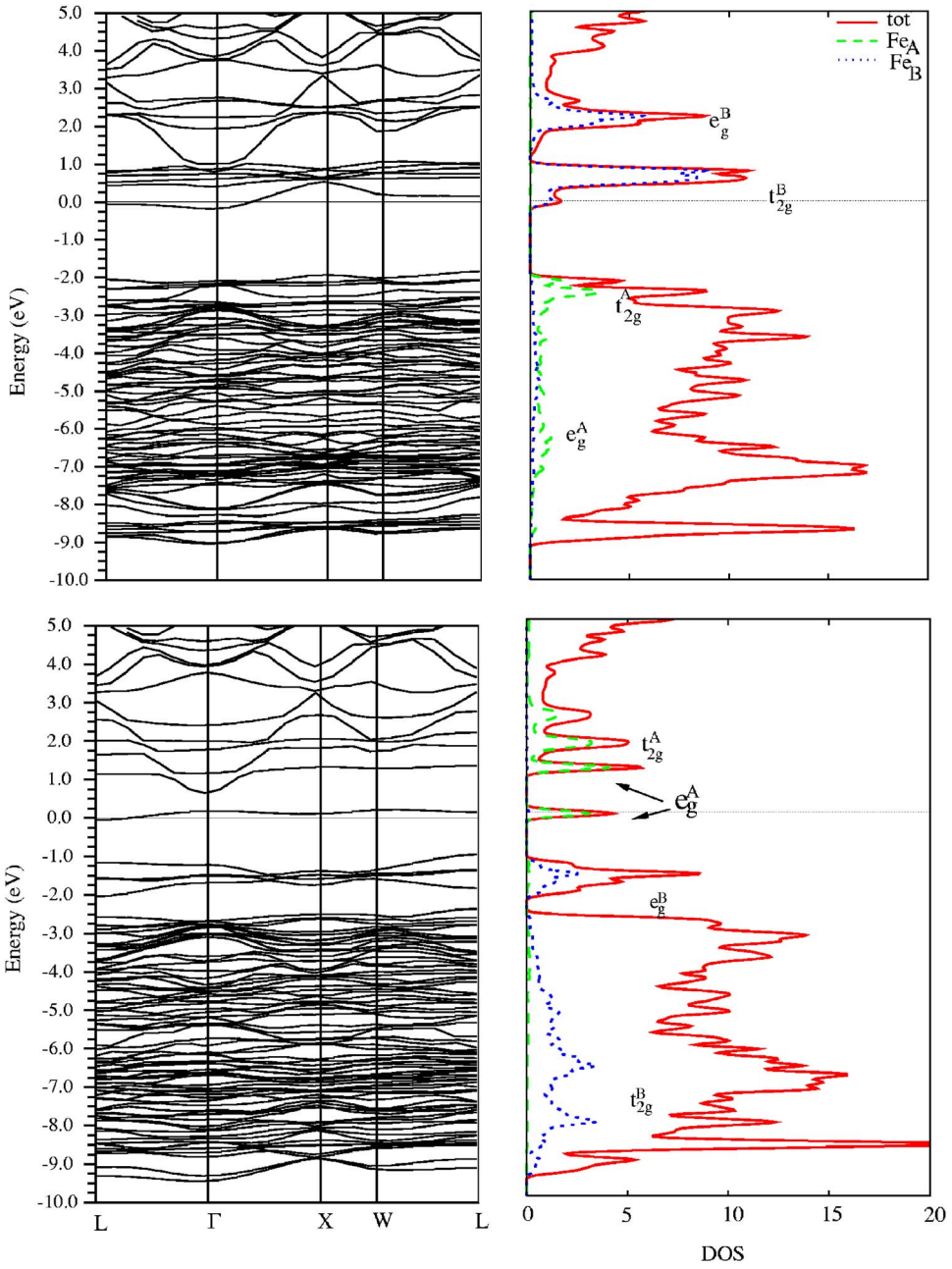

FIG. 8. (Color online) Band structure (left panel) and total and decomposed density of states (right panel) for the structure of case Fig. 5(ii) within LDA+U with $U=4.5$ eV and $J=1$ eV. Line description as in Fig. 6.

ground state which is a desirable property for spintronic applications. We observed that Fe doping in the *A* site could give rise to a spin-polarized current due to the presence of highly dispersive *s* band in one-spin channel. In the *B* site, Mn instead of Fe could lead to a half-metallic state by setting the Fermi level in a comparatively wider e_g band in the spin-up channel. Doping both *A* and *B* sites with Fe leads to a so-called "transport half-metal" when there is a direct Fe-Fe bonding in the *B* sites.

TABLE II. Comparison of forces on Fe and O atoms in structure (i) and (ii) (units mRy/a.u.).

	Fe_A	Fe_B	O
(i)	20.589	6.623	36.442
(ii)	40.395	9.240	60.324

Finally, recent work on $[ZnGa_2O_4]_{1-x}[Fe_3O_4]_x$ for various large Fe doping concentrations showed the existence of a ferromagnetic phase up to 200 K. Mössbauer spectra were measured and provided a quadrupolar splitting of 0.52 mm/s. Assuming a nuclear quadrupole moment for ^{57}Fe of 0.16 b, as calculated in Ref. 28 within the LAPW method, the resulting electric field gradient (EFG) is 3.12 V/cm^2. Alternatively, assuming a nuclear quadrupole moment of 0.2 b, as calculated in Ref. 29, the EFG is 2.5 V/cm^2. When Fe is substituted into an *A* site no EFG develops due to the spherical local symmetry at the nucleus. Instead, in the case of Fe doped into a *B* site the optimized structure provided us with an EFG at the Fe site of 2.11 V/cm^2, which compares fairly well with the experimental values. In the doping case of Fe

into *A* and *B* sites we did not perform a structure optimization, and since the EFG is quite sensitive to structural changes, we obtain quite different values with respect to the experimental ones.

The Mössbauer experiment of Risbud *et al.*[5] detected the presence of only Fe^{3+}. This result would discard the option of Fe doped in the *A* site in favor of Fe doped on the *B* site since from our calculations Fe in the *A* site takes up an oxidation state close to 2+ and not to 3+. In fact, in $ZnGa_2O_4$ the site preference of Zn^{2+} towards the tetrahedral sites is much stronger than the Fe one[30] and this can explain why Risbud *et al.* detected the presence of only Fe^{3+}, which probably occupies predominantly *B* sites. Alternatively, Mg^{2+} has a weaker preference for the *A* site than Ga and Fe; therefore, replacing Zn^{2+} with Mg^{2+} can provide a practically easier way to populate *A* sites with Fe and $MgGa_2O_4$ would be a better host candidate for the properties presented here concerning Fe doping on the *A* site.

ACKNOWLEDGMENTS

We would like to thank R. Seshadri for useful discussions and the German Science Foundation for financial support. We would also like to thank P. Blaha for helpful discussion regarding the code WIEN2k.

[1] S. A. Wolf, D. D. Awschalom, R. A. Buhrman, J. M. Daughton, S. von Molnar, M. L. Roukes, A. Y. Chtchelkanova, and D. M. Terger, Science **294**, 1488 (2001).
[2] H. Ohno, Science **281**, 951 (1998).
[3] J. Konig, J. Schliemann, T. Jungwirth, and A. H. MacDonald, cond-mat/0111314 (unpublished).
[4] S. J. Pearton, C. R. Abernathy, G. T. Thaler, R. M. Frazier, D. P. Norton, F. Ren, Y. D. Park, J. M. Zavada, I. A. Buyanova, W. M. Chen, and A. F. Hebard, J. Phys.: Condens. Matter **16**, R209 (2004); S. J. Pearton, W. H. Heo, M. Ivill, D. P. Norton, and T. Steiner, Semicond. Sci. Technol. **19**, R59 (2004).
[5] A. S. Risbud, R. Seshadri, J. Ensling, and C. Felser, J. Phys.: Condens. Matter **17**, 1003 (2005).
[6] A. Krimmel, Z. Seidov, G. G. Guseinov, A. I. Najafov, H.-A. Krug von Nidda, A. Loidl, and D. M. Többens, J. Phys.: Condens. Matter **17**, 3611 (2005).
[7] J. P. Perdew and Y. Wang, Phys. Rev. B **45**, 13244 (1992).
[8] J. P. Perdew, K. Burke, and M. Ernzerhof, Phys. Rev. Lett. **77**, 3865 (1996).
[9] P. Blaha, K. Schwartz, G. K. H. Madsen, D. Kvasnicka, and J. Luitz, WIEN2k, an augmented plane wave+local orbitals program for calculating crystal properties, K. Schwarz, Technical University Wien, Austria, 2001, ISBN 3-9501031-1-2.
[10] P. E. Blochl, O. Jepsen, and O. K. Andersen, Phys. Rev. B **49**, 16223 (1994).
[11] M. Josties, H. S. C. O'Neill, K. Bente, and G. Brey, Neues Jahrb. Mineral., Monatsh. **1995**, 273.
[12] C. M. Fang, C.-K. Loong, G. A. de Wijs, and G. de With, Phys. Rev. B **66**, 144301 (2002).
[13] F. D. Murnaghan, Proc. Natl. Acad. Sci. U.S.A. **30**, 244 (1944).
[14] R. Pandey, J. D. Gale, S. K. Sampath, and J. M. Recio, J. Am. Ceram. Soc. **82**, 3337 (1999).
[15] D. Levy, A. Pavese, A. Sani, and V. Pischedda, Phys. Chem. Miner. **28**, 612 (2001).
[16] S. K. Sampath and J. F. Cordaro, J. Am. Ceram. Soc. **81**, 649 (1998).
[17] S. K. Sampath, D. G. Kanhere, and R. Pandey, J. Phys.: Condens. Matter **11**, 3635 (1999).
[18] *International Tables for Crystallography*, edited by Th. Hahn (Kluwer Academic, Dordrecht, 2002).
[19] M. Nonaka, S. Matsushima, M. Mizuno, and C. Zu, Key Eng. Mater. **228–229**, 303 (2002).
[20] M. T. Czyzyk and G. A. Sawatzky, Phys. Rev. B **49**, 14211 (1994).
[21] V. I. Anisimov, I. V. Solovyev, M. A. Korotin, M. T. Czyzyk, and G. A. Sawatzky, Phys. Rev. B **48**, 16929 (1993).
[22] T. Maitra and R. Valenti, J. Phys.: Condens. Matter **17**, 7417 (2005).
[23] P. Bagno, O. Jepsen, and O. Gunnarsson, Phys. Rev. B **40**, 1997 (1989).
[24] D. J. Singh, M. Gupta, and R. Gupta, Phys. Rev. B **63**, 205102 (2001).
[25] J. S. Kouvel, Phys. Rev. **102**, 1490 (1956).
[26] M. El-shabasy, J. Magn. Magn. Mater. **172**, 188 (1997).
[27] B. Nadgorny, I. I. Mazin, M. Osofsky, R. J. Soulen, Jr., P. Broussard, R. M. Stroud, D. J. Singh, V. G. Harris, A. Arsenov, and Ya. Mukovskii, Phys. Rev. B **63**, 184433 (2001).
[28] Philipp Dufek, Peter Blaha, and Karlheinz Schwarz, Phys. Rev. Lett. **75**, 3545 (1995).
[29] D. W. Mitchell *et al.*, Phys. Rev. B **53**, 7684 (1996).
[30] A. Navrostky and O. J. Kleppa, J. Inorg. Nucl. Chem. **29**, 2701 (1967).